Zero Hall conductivity and its electronic origin in a Cr-doped topological insulator

Jeongwoo Kim, Yusheng Hou, Noejung Park, and Ruqian Wu

Phys. Rev. B **98**, 081117 — Published 31 August 2018

DOI: 10.1103/PhysRevB.98.081117

Zero Hall conductivity and its electronic origin in Cr-doped topological insulator

Jeongwoo Kim[1,2], Yusheng Hou[1], Noejung Park[2], & Ruqian Wu[1*]

[1]*Department of Physics and Astronomy, University of California, Irvine, California 92697, USA*

[2]*Department of Physics, Ulsan National Institute of Science and Technology, Ulsan 44919, Republic of Korea*

Abstract

We investigate the electronic origin of the zero Hall conductivity or the axion phase of a Cr-doped Sb_2Te_3 film by analyzing the evolution of its band structure upon the magnetic field sweep. By applying a small electric field or using asymmetric doping, we differentiate the coercivities of the two surfaces, so they can form either ferromagnetic (FM) or antiferromagnetic (AFM) alignment. Through the surface-resolved Berry curvature calculations, we demonstrate that the system manifests robust zero Hall plateaus when the two surfaces remain topologically nontrivial and enter a magnetic state which has intra-surface FM and inter-surface AFM orderings. Our results provide insights for the understanding of the uncharted issues of axion insulators, complementary to the exciting experimental progresses in this realm.

PACS: 75.50.Pp, 73.20.At, 73.43.Cd

Topological classification of matters has become a new way to comprehend emergent quantum phenomena in condensed matter physics ever since the discovery of the quantum Hall effect [1-3]. Three dimensional topological insulators (TIs), characterized by the coexistence of metallic helical surface states and insulating bulk states, are widely used for explorations of innovative quantum phenomena such as the quantum anomalous Hall (QAH) effect [4-12], large spin-orbit torque [13, 14], Majorana fermion [15-17], giant exchange interaction [18, 19], the topological magnetoelectric (TME) effect [20-24], and the quantized magneto-optical effect [24-29]. Although tremendous progress has been made for the realization of copious theoretical predictions in this realm, a clear demonstration of the TME effect is still in its formative stage due to the difficulty of finding a suitable axion insulator, in which the electric (magnetic) polarization is controlled by magnetic (electric) field owing to the topological θ term in the axion electrodynamics [22-24]. Therefore, searching for a stable axion insulator is an imperative multidisciplinary research task in order to exploit the fascinating TME responses of TIs in applications.

Recent studies showed that an axion insulator can be realized in Cr (or V)-doped (Sb, Bi)$_2$Te$_3$ [30-32], in which the asymmetric magnetic doping gives rise to different coercivities at the two surfaces. At the stage when the two magnetic layers align antiparallelly across the TI film, the sample simultaneously exhibits a zero Hall conductivity (σ_{xy}) and a vanishing longitudinal conductivity (σ_{xx}) [30]. The presence of the zero Hall plateau (ZHP) in a wide range of external magnetic field is a strong indication of an axion insulator [31, 32]. To eventually develop new axion insulators for technological innovations, it is crucial to explore 1) how the magnetic order and the band topology are intertwined; 2) what the electronic origin of ZHP is; and 3) how to control the magnetic anisotropy and magnetic orderings of TIs to expand the range of ZHP.

In this Letter, we discuss the physical mechanism of the zero Hall conductivity through the first-principles study of Cr-doped Sb_2Te_3. By constructing various magnetic configurations, the evolution of the band topology in response to the magnetic field sweep is systematically investigated. We show that the two surfaces have opposite Chern numbers when they form an antiferromagnetic order and remain topologically nontrivial, which leads to the formation of robust ZHP even in a thin TI film. We also find that a new type of the QAH effect driven by an asymmetric potential can be realized in two-dimensional limit. Our results unravel the mystery of the ZHP induced by magnetic modulation doping and provide a foundation for the development of axion insulators.

Our density functional theory calculations were carried out with the projected augmented plane-wave method [33, 34] as implemented in the Vienna *ab initio* simulation package (VASP) [35]. We constructed a slab model that is expanded to a (2×2) supercell in the lateral plane and has four quintuple layers (QLs) of Sb_2Te_3 and a 15 Å vacuum along the surface normal. We used the generalized gradient approximation for the description of exchange-correlation interaction among electrons [36], together with the van der Waals correction for a more accurate description of the long-range dispersion forces [37]. Spin-orbit coupling was included in the self-consistent calculations. The energy cutoff for the plane-wave expansion was chosen to be 300 eV. We adopted a 7×7×1 **k**-point grid to sample the Brillouin zone. Atomic relaxation was carried out until the change of total energy became less than 0.01 meV. The Chern numbers were evaluated from the Berry curvature [2, 38]

$$\Omega(\mathbf{k}) = -2\,\mathrm{Im}\sum_{n}\sum_{n'\neq n} f_n \frac{\langle \psi_{n\mathbf{k}} | v_x | \psi_{n'\mathbf{k}} \rangle \langle \psi_{n'\mathbf{k}} | v_y | \psi_{n\mathbf{k}} \rangle}{(\varepsilon_{n'\mathbf{k}} - \varepsilon_{n\mathbf{k}})^2}, \qquad (1)$$

where n is the band index, f_n is the Fermi-Dirac distribution function, $v_{x(y)}$ is the velocity operator, $\psi_{n\mathbf{k}}$ and $\varepsilon_{n\mathbf{k}}$ are the Bloch wave-function and eigenenergy of the n-th band at a **k**-

point, respectively. The Berry curvature is estimated from the maximally-localized Wannier function using the WANNIER90 package [39, 40].

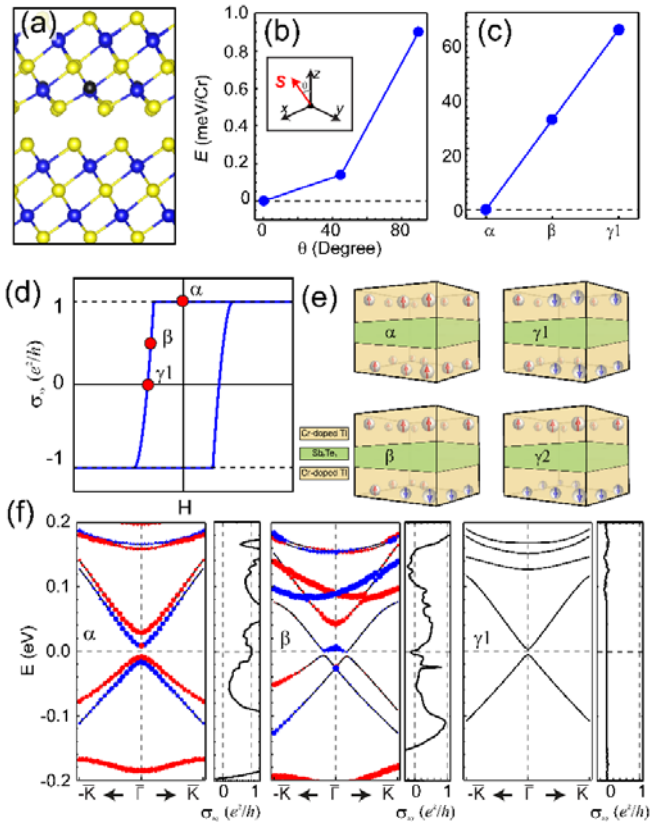

Figure 1. (a) Atomic structure of four-QL Cr-doped (6.25 %) Sb_2Te_3. Blue spheres, Sb; yellow spheres, Te; black spheres, Cr. (b) Energy variation of the ferromagnetic phase upon the magnetism direction. (c) Energy variation of Cr-doped Sb_2Te_3 upon the magnetic configuration (α, β, and γ1 phases). (b), (c) The total energy of the surface normal magnetism (α phase) is set to zero. (d) Schematic Hall conductivity (σ_{xy}) and (e) various magnetic configurations (α, β, γ1, and γ2 phases) of a symmetric Cr-doped TI thin film upon varying the magnetic field. (f) Calculated band structures and anomalous Hall conductivities (σ_{xy}) of four-QL Cr-doped (12.5 %) Sb_2Te_3 for the α, β, and γ1 phases. Spin-up (spin-down) states are marked by the red (blue) dots.

We first elucidate the dependence of electronic and topological properties of a symmetrically Cr-doped (12.5 % in a QL) TI film on the magnetic field sweep. As shown in Fig. 1a, Cr dopants are placed in the two outermost QLs to maximize the interaction between

the topological surface state and magnetic impurities [41]. We note Cr atoms are way from the surface in experiment by ~1nm (1 QL) [42], which leads to the maximal exchange splitting [43]. According to the scanning SQUID measurement and magnetic force microscopy image [32, 44], a homogenous ferromagnetic order of dopants leads to the QAH state (Chern number = 1) whereas a superparamagnetic order gives the trivial state (Chern number = 0). Here, we mimic the change of magnetic structure with three different magnetic configurations (*α, β,* and *γ1* as sketched in Fig. 1e) based on experimental findings and calculate their total energies. The ferromagnetic *α* state, with an easy axis along the surface-normal [Fig. 1b], is more stable than other mixed magnetic states [Fig. 1c]. As illustrated in Fig. 1d, the QAH effect was characterized by a quantized Hall conductivity along with a clear ferromagnetic hysteresis loop. To see the variation of the electronic structure of the QAH state upon the magnetic field sweep, we calculate their surface band structures and anomalous Hall conductivities for three different phases [Fig. 1f]. The signature of the QAH effect, *i.e.* the presence of Dirac surface states with both band inversion and spin splitting at the Fermi level, is reproduced in our calculations for the *α* phase. Furthermore, an integer value of the Hall conductivity near the Fermi level is obtained. When the ferromagnetic order in the bottom surface is destroyed (the *β* phase), the Dirac cone of the bottom surface is shifted down by -30 meV and its gap is also significantly reduced. In contrast, the Dirac cone of the top layer remains almost intact except the slight upshift to above the Fermi level. Interestingly, the Hall conductivity of the *β* phase becomes almost zero at the Fermi level and approaches a half integer in the band gap of the top surface (~0.05 eV). When the ferromagnetic order in both surfaces is destroyed as we further increase the magnetic field to the *γ1* phase in Fig. 1d, the anomalous Hall conductivity of the system completely disappears.

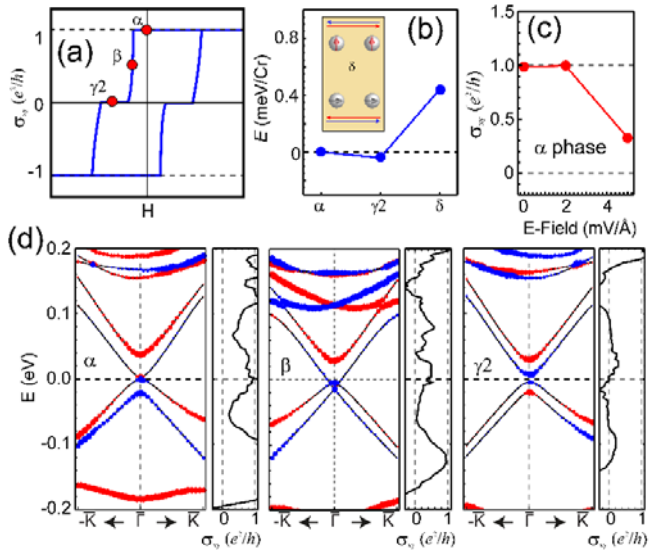

Figure 2. (a) Schematic Hall conductivity (σ_{xy}) of an asymmetric Cr-doped TI thin film upon varying magnetic fields. (b) The stability of the γ2 phases in comparison to the ferromagnetic state (α phase) and the intermixed artificial state (δ phase). The total energy of the surface normal magnetism (α phase) is set to zero. The inset is the schematic drawing for the δ phase (c) The variation of anomalous Hall conductivity (σ_{xy}) of the ferromagnetic α phase as a function of the electric field strength. (d) Calculated band structures and anomalous Hall conductivities (σ_{xy}) of four-QL Cr-doped Sb_2Te_3 for various magnetic configurations (α, β, and γ2 phases) when subjected to an electric field (2 mV/Å). Spin-up (spin-down) states are marked by the red (blue) dots.

From what we discussed above, it is obvious that one needs to break the inversion symmetry between the two surfaces to attain the ZHP. Here we apply an electric field along the perpendicular axis to produce such an asymmetry, by shifting states in the top and bottom surfaces oppositely with respect to the Fermi level. This may change the magnetic anisotropies of the two surfaces and hence they may have different coercivities. As we sweep the magnetic field, we now reach three magnetic configurations marked as *α, β,* and *γ2* in Fig. 2a. Here, the *γ2* phase has ferromagnetic orders at both surfaces but they are antiparallel to each other (cf. Fig. 1e), similar to what was obtained by the modulation doping in experiments [30]. We also examine the stability of the *γ2* phase [Fig. 2b]. The *γ2* phase is

energetically as stable as the α phase, which shows the validity of our magnetic model. Fig. 2c shows that the anomalous Hall conductivity of the α phase is quantized until the electric field reaches up to 2 mV/Å and the nontrivial topology is destroyed if the electric field further increases. Under this critical electric field (2 mV/Å), the overall electronic structures of the α and β phases are very similar to those without the electric field displayed in Fig. 1. The *γ2* phase indeed has the zero-Hall state at the Fermi level, as shown in Figs. 2d and Fig. S1 [45]. However, the Hall conductivity quickly becomes nonzero away from the Fermi level and spin splittings can be found in the band structure, sharply different from the *γ1* phase. Since the Fermi level lies right in the band gap, the longitudinal conductivity (σ_{xx}) should also vanish, fulfilling the requirements for the axion state. One thing interesting is if the asymmetric potential surpasses the weak perturbation regime (field > 2 mV/Å), the ZHP disappears but a new QAH state may emerge (Figs. S2 and S3) [45] in the four-QL Cr-doped Sb_2Te_3 film. The robust QAH state is driven by the quantum confinement effect without the band inversion of topological surface states [4, 46-48]. Consequently, the asymmetric QAH effect, irrelevant to the topological surface states, is likely to persist in higher temperature since the small exchange splitting of topological surface states is identified as the main reason for the extremely low characteristic temperature of the QAH effect [47].

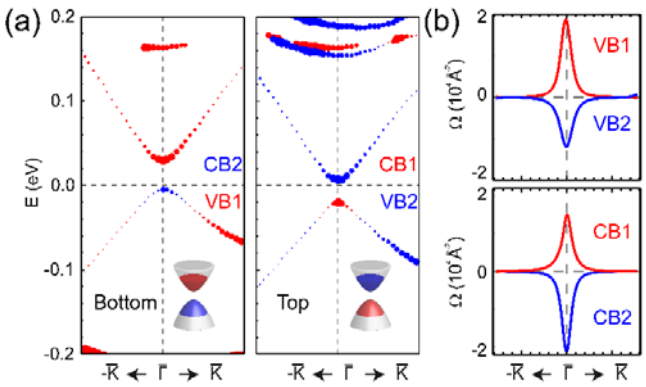

Figure 3. (a) Site-projected band structures (top and bottom QLs) and (b) the Berry curvature

of states near the Fermi level. Spin-up (spin-down) states are marked by the red (blue) dots. VB (CB) stands for valence(conduction) band.

To better understand the ZHP, we resolve electronic bands of the *γ2* phase to the top and bottom surfaces. The relative energy shift of states in the top and bottom surfaces caused by the electric field is clearly shown in Fig. 3a and, their spin components are opposite. The finite Hall conductivity near the Fermi level can be attributed to the non-zero Berry curvature of conduction and valence bands around the Γ point [Fig. 3b]. Interestingly, the conduction band minima (CB1, in the top surface) and the valence band maxima (VB1, in the bottom surface) have the same spin component and Berry curvature (Fig. 3b), implying that the *γ2* phase is robust against external perturbation on the electronic structure near the Fermi level. Although the Chern numbers of the two surfaces are exactly canceled out in the *γ2* phase, the Berry curvatures of both VB1 and VB2 are nonzero (Fig. 3b). We also explicitly confirm the opposite half-Chern numbers using a simple model Hamiltonian [45]. Therefore, we have the half-integer quantum Hall effect on each surface as deduced from the flow diagram of (σ_{xx}, σ_{xy}) in experiment [12, 32]. Obviously, the key ingredients for magnetic TIs to enter the state of an axion insulator are (1) preserving the topological nature of two surfaces and (2) having the magnetic configuration as depicted in Fig. 1e for the *γ2* phase.

To test if the zero-Hall state is robust against the presence of an external magnetic field which is needed to set the system to the *γ2* phase, we added a Zeeman field in our calculations while the antiparallel magnetic order is kept between the two surfaces. The Zeeman field was set to 10 meV, which is excessively large but is needed to reproduce the perturbation which severely changes the electronic structure. As shown in Fig. 4a, the zero-Hall effect of the *γ2* phase is well protected even in this strong magnetic field. In contrast, the *γ1* phase shows nonzero Hall conductivity in Fig. 4b, and its sign flips with the direction

switch of the magnetic field as expected for ordinary materials.

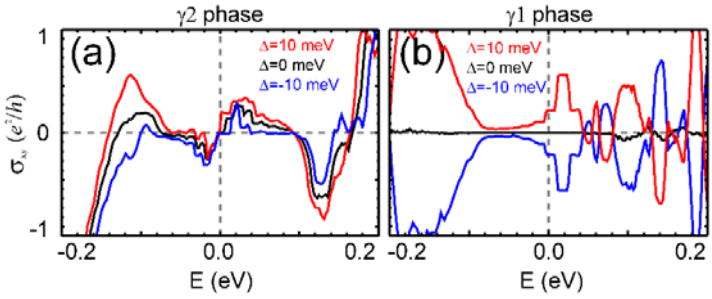

Figure 4. The variation of anomalous Hall conductivity (σ_{xy}) of (a)the γ2 and (b) γ1 phases upon the Zeeman splitting (Δ) from -10 meV to 10meV.

We find that the ZHP can also be obtained by adjusting the depth of Cr dopants in Sb_2Te_3 thin film. Obviously, magnetic properties of Cr dopants should depend on their vertical position. In Fig. 5, we see that magnetic anisotropy energy (MAE, defined as the energy difference as the magnetization switches from the in-plane to the surface-normal direction) changes in a rather large range as Cr atoms are moved to different locations. Magnetic impurities in the outermost QL experience lower symmetry and an additional spin-orbit coupling carried by the topological surface states, both lead to the enhancement of the MAE at the surface [19]. The strong MAE~z dependence allows that local spins of magnetic impurities in two surfaces are flipped separately to enter the *γ2* phase, depending on their depths in implementation for the top and bottom surfaces [30].

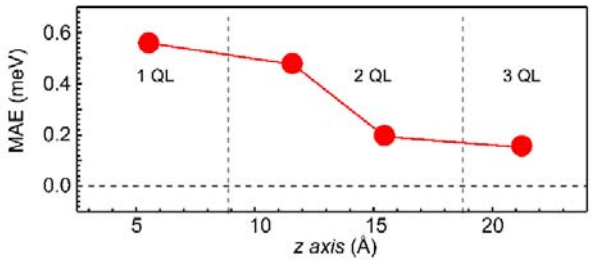

Figure 5. Calculated magnetic anisotropy energy (MAE) of five-QL Cr-doped Sb_2Te_3 for

varying the Cr position from outside to inside. The position of the outermost Te layers is set to 0.

Up to now, it is believed that a thick spacer (~5 QLs) is required to decouple the two surfaces for making axion insulators. According to our calculations (Figs. 1 and S4), the inter-surface exchange energy is less than 0.1 meV, which indicates the two-QL thickness of Sb_2Te_3 is enough to cut off the exchange interaction. Based on this work, we see that two different ways may produce the ZHP even in very thin films by changing the inter-surface exchange interaction. In the two-dimensional limit (or very thin limit), the mass gap of Dirac cones becomes larger due to their inter-surface coupling and consequently the ZHP might be observable via gate voltage tuning at higher temperature. Another advantage of thin thickness is that the insulating nature is more easily attained by avoiding the band crossing through inter-surface coupling. As discussed above, the ZHP is a rather robust feature in a thin film if two surfaces have different MAEs. Therefore, we may introduce a ferromagnetic or antiferromagnetic insulator on top of one of the surfaces to change the MAE of Cr dopants. To this end, extensive studies have already been done, using EuS [18], yttrium iron garnet [49], and MnSe [50]. The unwanted damage of topological surface states due to the interfacial hybridization can be remediated by inserting Te capping layers on TIs [32]. Recently discovered two-dimensional van der Waals ferromagnet CrI_3 monolayer are also promising [51].

Another key aspect for entering the *γ2* phase is the reduction of exchange interaction between top and bottom surfaces. Even if we use different magnetic dopants such as Cr and V to produce different coercive fields, the exchange interaction between two surfaces may nullify their distinction or reduce the length of the plateau. One may insert a buffer layer in TIs to reduce the magnetic exchange interaction between the two surfaces. For example,

Sb_2Se_3 shares the similar atomic and electronic structure with Sb_2Te_3, but the exchange interaction becomes weaker by using smaller anion atoms that mediate the exchange interaction in magnetic TIs (Fig. S4) [45-47]. Using the state-of-art molecular beam epitaxy technique, these fine structure engineering should be doable [12, 30, 32]. With this insertion, the zero-Hall state is stable in a wider range of magnetic field in the two-dimensional limit (Fig. S4) [45].

To summarize, we showed that the antiparallel magnetic order between the surfaces of a Sb_2Te_3 film can be created by differentiating the coercivities of Cr dopants. The exotic zero-Hall phase, a strong signature of axion insulator, is developed by a small electric field or modulation doping as well as the QAH phase. We demonstrated that the robust ZHP originates from the nontrivial band topology through the surface-resolved Berry curvature calculations. We also proposed some possible ways to attain the ZHP, with a stacked magnetic insulator or an inserted buffer layer, in thin TI films. Our results for a real material system fill the gap between model analyses and the experimental observation and the new physical insights should be very useful for guiding the design of axion insulators.

This work was support by DOE-BES (Grant No. DE-FG02-05ER46237). Calculations were performed on parallel computers at NERSC supercomputer centers. JK and NP acknowledge the support from BRL (NRF-2017R1A4A101532).

References

[1] K. v. Klitzing, G. Dorda, and M. Pepper, Phys. Rev. Lett. **45**, 494 (1980).

[2] D. J. Thouless, M. Kohmoto, M. P. Nightingale, and M. den Nijs, Phys. Rev. Lett. **49**, 405 (1982).

[3] F. D. M. Haldane, Phys. Rev. Lett. **61**, 2015 (1988).

[4] R. Yu, W. Zhang, H.-J. Zhang, S.-C. Zhang, X. Dai, and Z. Fang, Science **329**, 61 (2010).

[5] C.-Z. Chang, J. Zhang, X. Feng, J. Shen, Z. Zhang, M. Guo, K. Li, Y. Ou, P. Wei, L.-L. Wang, Z.-Q. Ji, Y. Feng, S. Ji, X. Chen, J. Jia, X. Dai, Z. Fang, S.-C. Zhang, K. He, Y. Wang, L. Lu, X.-C. Ma, and Q.-K. Xue, Science **340**, 167 (2013).

[6] J. G. Checkelsky, R. Yoshimi, A. Tsukazaki, K. S. Takahashi, Y. Kozuka, J. Falson, M. Kawasaki, and Y. Tokura, Nat. Phys. **10**, 731 (2014).

[7] X. Kou, S.-T. Guo, Y. Fan, L. Pan, M. Lang, Y. Jiang, Q. Shao, T. Nie, K. Murata, J. Tang, Y. Wang, L. He, T.-K. Lee, W.-L. Lee, and K. L. Wang, Phys. Rev. Lett. **113**, 137201 (2014).

[8] A. J. Bestwick, E. J. Fox, X. Kou, L. Pan, K. L. Wang, and D. Goldhaber-Gordon, Phys. Rev. Lett. **114**, 187201 (2015).

[9] C.-Z. Chang, W. Zhao, D. Y. Kim, P. Wei, J. K. Jain, C. Liu, M. H. W. Chan, and J. S. Moodera, Phys. Rev. Lett. **115**, 057206 (2015).

[10] C.-Z. Chang, W. Zhao, D. Y. Kim, H. Zhang, B. A. Assaf, D. Heiman, S.-C. Zhang, C. Liu, M. H. W. Chan, and J. S. Moodera, Nat. Mater. **14**, 473 (2015).

[11] S. Grauer, S. Schreyeck, M. Winnerlein, K. Brunner, C. Gould, and L. W. Molenkamp, Phys. Rev. B **92**, 201304 (2015).

[12] S. Grauer, K. M. Fijalkowski, S. Schreyeck, M. Winnerlein, K. Brunner, R. Thomale, C. Gould, and L. W. Molenkamp, Phys. Rev. Lett. **118**, 246801 (2017).

[13] Y. Fan, P. Upadhyaya, X. Kou, M. Lang, S. Takei, Z. Wang, J. Tang, L. He, L.-T. Chang, M. Montazeri, G. Yu, W. Jiang, T. Nie, R. N. Schwartz, Y. Tserkovnyak, and K. L. Wang, Nat. Mater. **13**, 699 (2014).

[14] Y. Fan, X. Kou, P. Upadhyaya, Q. Shao, L. Pan, M. Lang, X. Che, J. Tang, M. Montazeri, K. Murata, L.-T. Chang, M. Akyol, G. Yu, T. Nie, K. L. Wong, J. Liu, Y. Wang, Y. Tserkovnyak, and K. L. Wang, Nat. Nanotechnol. **11**, 352 (2016).

[15] L. Fu, and C. L. Kane, Phys. Rev. Lett. **100**, 096407 (2008).

[16] X.-L. Qi, and S.-C. Zhang, Rev. Mod. Phys. **83**, 1057 (2011).

[17] Q. L. He, L. Pan, A. L. Stern, E. C. Burks, X. Che, G. Yin, J. Wang, B. Lian, Q. Zhou, E. S. Choi, K. Murata, X. Kou, Z. Chen, T. Nie, Q. Shao, Y. Fan, S.-C. Zhang, K. Liu, J. Xia, and K. L. Wang, Science **357**, 294 (2017).

[18] F. Katmis, V. Lauter, F. S. Nogueira, B. A. Assaf, M. E. Jamer, P. Wei, B. Satpati, J. W. Freeland, I. Eremin, D. Heiman, P. Jarillo-Herrero, and J. S. Moodera, Nature **533**, 513 (2016).

[19] J. Kim, K.-W. Kim, H. Wang, J. Sinova, and R. Wu, Phys. Rev. Lett. **119**, 027201 (2017).

[20] A. M. Essin, J. E. Moore, and D. Vanderbilt, Phys. Rev. Lett. **102**, 146805 (2009).

[21] K. Nomura, and N. Nagaosa, Phys. Rev. Lett. **106**, 166802 (2011).

[22] J. Wang, B. Lian, X.-L. Qi, and S.-C. Zhang, Phys. Rev. B **92**, 081107 (2015).

[23] T. Morimoto, A. Furusaki, and N. Nagaosa, Phys. Rev. B **92**, 085113 (2015).

[24] X.-L. Qi, T. L. Hughes, and S.-C. Zhang, Phys. Rev. B **78**, 195424 (2008).

[25] J. Maciejko, X.-L. Qi, H. D. Drew, and S.-C. Zhang, Phys. Rev. Lett. **105**, 166803 (2010).

[26] W.-K. Tse, and A. H. MacDonald, Phys. Rev. Lett. **105**, 057401 (2010).

[27] K. N. Okada, Y. Takahashi, M. Mogi, R. Yoshimi, A. Tsukazaki, K. S. Takahashi, N. Ogawa, M. Kawasaki, and Y. Tokura, Nat. Commun. **7**, 12245 (2016).

[28] L. Wu, M. Salehi, N. Koirala, J. Moon, S. Oh, and N. P. Armitage, Science **354**, 1124 (2016).

[29] V. Dziom, A. Shuvaev, A. Pimenov, G. V. Astakhov, C. Ames, K. Bendias, J. Böttcher, G. Tkachov, E. M. Hankiewicz, C. Brüne, H. Buhmann, and L. W. Molenkamp, Nat. Commun. **8**, 15197 (2017).

[30] M. Mogi, M. Kawamura, R. Yoshimi, A. Tsukazaki, Y. Kozuka, N. Shirakawa, K. S. Takahashi, M. Kawasaki, and Y. Tokura, Nat. Mater. **16**, 516 (2017).

[31] M. Mogi, M. Kawamura, A. Tsukazaki, R. Yoshimi, K. S. Takahashi, M. Kawasaki, and Y. Tokura, Sci. Adv. **3**, eaao1669 (2017).

[32] D. Xiao, J. Jiang, J.-H. Shin, W. Wang, F. Wang, Y.-F. Zhao, C. Liu, W. Wu, M. H. W. Chan, N. Samarth, and C.-Z. Chang, Phys. Rev. Lett. **120**, 056801 (2018).

[33] P. E. Blöchl, Phys. Rev. B **50**, 17953 (1994).

[34] G. Kresse, and D. Joubert, Phys. Rev. B **59**, 1758 (1999).

[35] G. Kresse, and J. Hafner, Phys. Rev. B **49**, 14251 (1994).

[36] J. P. Perdew, K. Burke, and M. Ernzerhof, Phys. Rev. Lett. **77**, 3865 (1996).

[37] A. Tkatchenko, and M. Scheffler, Phys. Rev. Lett. **102**, 073005 (2009).

[38] Y. Yao, L. Kleinman, A. H. MacDonald, J. Sinova, T. Jungwirth, D.-s. Wang, E. Wang, and Q. Niu, Phys. Rev. Lett. **92**, 037204 (2004).

[39] A. A. Mostofi, J. R. Yates, Y.-S. Lee, I. Souza, D. Vanderbilt, and N. Marzari, Comput. Phys. Commun. **178**, 685 (2008).

[40] J. Kim, J. Kim, Y.-S. Song, R. Wu, S.-H. Jhi, and N. Kioussis, Phys. Rev. B **96**, 235304 (2017).

[41] J. Kim, and S.-H. Jhi, Phys. Rev. B **92**, 104405 (2015).

[42] M. Mogi, R. Yoshimi, A. Tsukazaki, K. Yasuda, Y. Kozuka, K. S. Takahashi, M. Kawasaki, and Y. Tokura, Appl. Phys. Lett. **107**, 182401 (2015).

[43] V. N. Men'shov, V. V. Tugushev, and E. V. Chulkov, JETP Lett. **104**, 453 (2016).

[44] E. O. Lachman, M. Mogi, J. Sarkar, A. Uri, K. Bagani, Y. Anahory, Y. Myasoedov, M. E. Huber, A. Tsukazaki, M. Kawasaki, Y. Tokura, and E. Zeldov, npj Quantum Materials **2**, 70 (2017).

[45] See Supplemental Material at […] for the robustness of the zero-Hall phase, the effect of asymmetric Cr doping on the electronic structure, the effect of the buffer layer Sb2Se3,and the model Hamiltonian results.

[46] J. Kim, H. Wang, and R. Wu, Phys. Rev. B **97**, 125118 (2018).

[47] J. Kim, S.-H. Jhi, A. H. MacDonald, and R. Wu, Phys. Rev. B **96**, 140410 (2017).

[48] J. Kim, S.-H. Jhi, and R. Wu, Nano Lett. **16**, 6656 (2016).

[49] Y. T. Fanchiang, K. H. M. Chen, C. C. Tseng, C. C. Chen, C. K. Cheng, S. R. Yang, C. N. Wu, S. F. Lee, M. Hong, and J. Kwo, Nat. Commun. **9**, 223 (2018).

[50] T. Hirahara, S. V. Eremeev, T. Shirasawa, Y. Okuyama, T. Kubo, R. Nakanishi, R. Akiyama, A. Takayama, T. Hajiri, S.-i. Ideta, M. Matsunami, K. Sumida, K. Miyamoto, Y. Takagi, K. Tanaka, T. Okuda, T. Yokoyama, S.-i. Kimura, S. Hasegawa, and E. V. Chulkov, Nano Lett. **17**, 3493 (2017).

[51] B. Huang, G. Clark, E. Navarro-Moratalla, D. R. Klein, R. Cheng, K. L. Seyler, D. Zhong, E. Schmidgall, M. A. McGuire, D. H. Cobden, W. Yao, D. Xiao, P. Jarillo-Herrero, and X. Xu, Nature **546**, 270 (2017).